Arabian Journal of Chemistry (2021) **14**, 103118

King Saud University

Arabian Journal of Chemistry

www.ksu.edu.sa
www.sciencedirect.com

ORIGINAL ARTICLE

Multifeatured guar gum armed drug delivery system for the delivery of ofloxacin drug to treat ophthalmic dieases

Qiang Shi [a], E.R. Anishiya Chella Daisy [b], GeqiangYang [c], Jing Zhang [c], Suresh Mickymaray [d], FaizAbdulaziz Alfaiz [d], Anand Paramasivam [e], Mariappan Rajan [b,*]

[a] *Department of Ophthalmology, The First Affiliated Hospital of Xi'an Jiao Tong University, Xi'an 710061, China*
[b] *Biomaterials in Medicinal Chemistry Laboratory, Department of Natural Products Chemistry, School of Chemistry, Madurai Kamaraj University, Madurai 625021, Tamil Nadu, India*
[c] *Department of Ophthalmology, Xi'an Central Hospital, No. 161 of Xiwu Road, Xincheng District, Xi'an, Shaanxi 710003, China*
[d] *Department of Biology, College of Science, Al-Zulfi, Majmaah University, Majmaah 11952, Riyadh region, Saudi Arabia*
[e] *Department of Basic Medical Sciences, College of Dentistry, Al-Zulfi, Majmaah University, Majmaah 11952, Riyadh Region, Saudi Arabia*

Received 8 January 2021; accepted 7 March 2021
Available online 21 March 2021

KEYWORDS

Biotin;
Guar gum;
Ofloxacin;
Opthalmatic treatment;
Polycaprolactone;
Targeted delivery

Abstract Nanotargeting delivery system is recently much more attention for delivering drugs and bioactive compounds to treating ocular diseases. Here, the Guar gum (GG) armed drug delivery system with functionalization of poly-caprolactone (PCL), Retinol (RA), Biotinylated-Glutathione (B-GHS), carried out by the condensation reactions. The functional changes and crystallinity of the prepared micelle system were characterized by the FTIR and XRD techniques. The SEM observation represents the morphology of micelle GG-g-PCL-RA-B-GHS; it shows sphere-like morphology, and it was correlated with TEM results. The unloaded and drug-loaded micelle's average spherical diameter was found as ~4.5 and ~6.8 nm, respectively, by the ImageJ software analysis. The carrier systems' surface charge was found as a negative value from zeta potential analysis. From in-vitro drug release studies, the drug release in a tear fluid environment (PBS, pH 7.4) was observed 88.0% of OFL in 8 h, and the drug release rate renewed in a controlled manner leads to the requirement for prolonged drug delivery. The antibacterial activity, the incubation of OFL loaded GG-g-PCL-RA-B-GHS micelle groups, found an excellent antibacterial activity against

* Corresponding author.
E-mail address: rajanm153.chem@mkuniversity.org (M. Rajan).
Peer review under responsibility of King Saud University.

Production and hosting by Elsevier

https://doi.org/10.1016/j.arabjc.2021.103118
1878-5352 © 2021 The Author(s). Published by Elsevier B.V. on behalf of King Saud University.
This is an open access article under the CC BY-NC-ND license (http://creativecommons.org/licenses/by-nc-nd/4.0/).

both gram-negative *Salmonella Typhi* and gram-positive *Bacillus cereus*. Since the novel OFL loaded GG-g-PCL-RA-B-GHS maintaining a prominent role in the delivery of OFL and good antibacterial activity, it could be offered as a promising strategy for ocular drug delivery.

© 2021 The Author(s). Published by Elsevier B.V. on behalf of King Saud University. This is an open access article under the CC BY-NC-ND license (http://creativecommons.org/licenses/by-nc-nd/4.0/).

1. Introduction

Ocular drug delivery is one of the fascinating methodologies but challenging route of drug administration (Djamila et al., 2013). In particular, Topical drug delivery into the eyes is the most popular and accessible route of administration to treat various eye diseases (Gaudana et al., 2010). The case of conventional eye drops accounts for more than 90% of the available ophthalmic formulations. These products' efficiency is limited by transient residence time, low permeability of corneal epithelium, rapid pre-corneal loss, and high tear fluid turnover of the eye are challenging and should be overcome drug to reach the tissue target (Agrahari et al., 2016). On the otherhand, one of the major drawbacks of conventional ophthalmic drugdelivery is the low drug bioavailability because of ocular anatomical and physiological constraints (Patel et al., 2013; Sahoo et al., 2008). The use of bioadhesive polymers can increase the residence time in the ocular region. Various polymeric nano-formulations have been explored to enhance drug retention and permeation (Khare et al., 2014; Jitendra et al., 2020). These are widely accepted due to their biodegradable and non-toxic nature. The different polymers are used for ocular polymeric nanoparticles, i.e., guar gum, eudragit RS-100, polycaprolactone (PCL), sodium alginate, pectin, chitosan, and galactomannan (Priyanka et al., 2012; Bhowmik et al., 2013). Guar gum (GG) is a well-known and most prominently used polymer in different ocular delivery systems. Moreover, guar gum has a substantial bioadhesive property and overcomes the rapid elimination from the ocular region by increasing the corneal contact time. It has shown promising results in ocular delivery due to the longer corneal surface retention (Soppimath et al., 2001; Kushwaha et al., 2012). The first generation of mucoadhesive polymers was able to form just weak non-covalent bonds such as hydrogen bonds to the mucus gel layer covering ocular surfaces, which increase the residence time of the drug (Leichner et al., 2019). Since guar gum-based micelle system will increase the residence time.

Similarly, synthetic polycaprolactone (PCL) has attained great importance lately because of its biocompatibility and biodegradability with the hydrophobic nature (Wang et al., 2020). The PCL has been reported to possess controlled drug release, optimum drug loading capability, with excellent stability (Song et al., 2018). The PCL has also been investigated as a nanofibrous scaffold for ocular surface reconstruction (Kong and Mi, 2016). Moreover, Targeted drug delivery could overcome conventional administration routes' deficiencies and enhance permeability (Li et al., 2016). Biotin increased the uptake and the transfer of carrier across retina endothelial cells (Ohkura, et al., 2010). Glutathione serves as a strong intracellular antioxidant and plays an essential role in protecting the eye from oxidative stress (Tan et al., 2018). Moreover, as a component of the NADPH pathway, it prevents cell components from being oxidized, thus promoting DNA regulation and protein synthesis (Ganea and Harding, 2006). Biotinylated glutathione could further increase carrier permeability through endothelial monolayers supporting its use as a cell targeting vector (XiuRen et al., 2015).

Retinol (Vitamin A) has a role in helping the rods in our eyes convert light into neuronal impulses for our brain. It is required to maintain the cornea and conjunctival membranes' normal differentiation, preventing other abnormal eye conditions (Arlappa, 2011). The lack of vitamin A in corneal tissues can result in abnormal differentiation of epithelial cells, resulting in keratinization, ulceration, epithelial squamous metaplasia, and a deficit of conjunctival goblet cells. As an important public health problem in many developing countries, Vitamin A deficiency triggered many studies on the use of retinoids for ocular surface diseases (Blomhoff, 1991; Sommer, 1983; Algahtani et al., 2020).

The present study aimed to develop novel combined delivery systems that synergistically associate the advantages of micelles and contribute to an even higher therapeutic effect. Micelle can offer to deliver vitamins, growth factors, and the antibiotic drug ofloxacin, one of the most widely used fluoroquinolones antibacterial agents, highly active against Gram-positive and Gram-negative bacteria. It is also active against mycoplasma, chlamydia, and legionella. The mechanism of the bactericidal effect of OFL is based on the inhibition ofthe bacteria's DNA gyrase. The enzyme produces anegative supercoil in DNA and thus permits transcription and replication (Sharma and Sahu, 2017; UstundagOkur et al., 2014).

In this regard, the co-polymeric guar gum grafted polycaprolactone (GG-g-PCL) segment's end-group can be readily modified with ligands and retinol. Here, targeting ligand as biotinylated glutathione can recognize cell-specific surface receptors, providing cellular selectivity and superior intracellular delivery to polymeric micelles. The retinol supplement plays an essential role in epithelial growth and limbal stem cell differentiation (Tan et al., 2016). Therefore, it promotes corneal wound healing, and OFL drugs act against bacterial keratitis. Thus the prepared OFL drug-loaded GG-g-PCL-RA-B-GHS polymeric micelle formulation can be used for the topical ocular treatment of bacterial keratitis and performed to enhance targeting and prolonging adherence at the eye surface.

2. Materials and methods

2.1. Materials

Guar gum (GG), ε-caprolactone (ε-CL), retinoic acid (RA), sodium borohydride, stannous octoate ($Sn(Oct)_n$), sodium citrate, biotin, glutathione, ofloxacin, toluene, dimethyl sulfoxide, ethanol, dimethylformamide, phosphate-buffered saline (PBS) solutions were purchased from Sigma-Aldrich, Chennai, India. Analytical-grade chemicals were purchased for all the experimentations. Without any further purification, the

chemicals were used. The deionized water was used in all the experiments.

2.2. Synthesis of guar gum grafted poly-caprolactone (GG-g-PCL)

Microwave-assisted co-polymerization of ε-CL in the —OH group of the GG was carried through the microwave oven at model MES-1000 purchased from CEM Corporation. It delivers selectable power up to 950 W at a frequency of 2.45 GHz at full Power (Tiwari and Prabaharan, 2010). Initially, 1.0 g GG was placed in a dried glass vessel, and PCL (2 g) was dissolved in 5 mL ethanol, and stannous octoate (1.0 mol) was added. The vessel was sealed under N_2 gas and stored overnight. After that, the vessel was irradiated under a microwave oven at 550 W microwave powers for 10 min. The obtained product was repeatedly washed with water and soxhlet extracted with methanol for 48 h to remove the homo-polymer of PCL. Finally, the GG-g-PCL was characterized for confirmation, and it was used for further carrier development.

2.3. Conjugation of RA in GG-g-PCLcopolymer

A condensation reaction in the GG-g-PCL polymer by RA was carried out by previously reported literature followed it with slight modifications (Anishiya Chella Daisy, 2020) The GG-g-PCL and RA in the molar ratios of 1:1 were mixed in deionized water in which approximate volume of toluene was placed in a 100 mL round bottom flask with Dean-Stark apparatus. Then Sn $(Oct)_n$ (0.1 mL) was added drop-wise, and the reaction mixture was heated at 110 °C for 24 h to reflux the mixture with continuous stirring and removal of water. The reaction mixture was cooled at room temperature (27 °C). The precipitate was filtered using Whatman filter paper and dried in a vacuum at room temperature. Further, the chemical structure of the RA conjugated GG-g-PCL copolymer confirmed via FT-IR spectroscopy.

2.4. Preparation of GG-g-PCL-RA-B-GHS

Before the grafting of B-GSH in the GG-g-PCL-RA, the GHS was conjugated with the biotin. The bond formation with biotin and glutathione was carried out via standard amide bond formation using EDC and NHS as the coupling reagents (Rajan et al., 2018). Typically, EDC (0.452 g) and NHS (0.257 g) were added to Biotin (0.6 g) in 5 mL of DMF at 0 °C for 15 min for activation of the carboxylic group. Then, the mixture was stirred at room temperature (27 °C) for 1 h. After 1 h, the resulting solution was adjusted to pH 6.0 using 1 M acetic acid and 1 M NaOH solution. The GSH (1 g, 6 mmol) solution was prepared in 5 mL of DMF solution and it was added to the above explanation; the reaction was carried out for 24 h at room temperature. The reaction mixture's pH was adjusted to pH 7.4 using 1 M acetic acid and 1 M NaOH solution, 2 h at room temperature. The obtained productwas then precipitated with cold diethyl ether, filtered, washed with diethyl ether. Finally, the solution was purified by dialysis (12000 kDa molecular weight cut-off [MWCO], Himedia, Mumbai, India) against distilled water for 48 h, and then lyophilized (Sub Zero Lyophilizer, Chennai, India) in −40 °C.

Further, the condensation reaction of B-GHS and GG-g-PCL-RA polymer was carried out, and the previously reported literature followed it with slight modifications (Anishiya Chella Daisy, 2020). The GG-g-PCL-RA (0.2 g) and B-GHS (0.2 g) in the molar ratios of 1:1 were mixed in deionized water, and which approximate volume of toluene was placed in a 100 mL round bottom flask with Dean-Stark apparatus. Then $Sn(Oct)_n$ (0.1 mL) was added drop-wise, and the reaction mixture was heated at 120 °C for 24 h to reflux the mixture with continuous stirring and removal of water. The reaction mixture was cooled at room temperature (27 °C), and the precipitate was filtered using Whatman filter paper and dried in a vacuum.

2.5. Preparationof OFL loaded GG-g-PCL-RA-B-GHS micelle

The OFL loaded GG-g-PCL-RA-B-GHS micelle was prepared using the membrane dialysismethod. Scheme 1 shows the graphical representation of micelle formation. Briefly, the GG-g-PCL-RA-B-GHS micelle (50 mg) and OLF (5 mg) were dissolved in 5 mL DMSO under stirring. With this mixture, 15 mL of deionized water was added drop-wise. After that, the mixture was dialyzed against deionized water using a dialysis tube (molecular mass cut-off 2 kDa) for 48 h. After that, the micelles were freeze-dried in an SSIPL-LYF Freeze drier frozen at −40 °C. A similar procedure was followed to prepare the free GG-g-PCL-RA-B-GHS micelles without using the OLF drug. All the prepared samples were sterilized by ultraviolet irradiation before biological characterization. The obtained product yield was provided in Table 1. The product yield percentage of the carrier was calculated through the following relationship:

$$\text{Product yield}(\%) = \frac{\text{Weight of the final product}}{\text{Total weight of the polymers}} \times 100$$

2.6. FT-IR analysis

The sample (10 mg) was placed on a holder and transferred to an FT-IR spectrometer (PerkinElmer Spectrum 100 series). The wavenumber range for FT-IR measurements was 4000–500 cm^{-1}, while the resolution ~4 cm^{-1} and the number of scans ~32.

2.7. Zeta potential and particle size analysis

The zeta potential was measured using dispersed solutions of the samples with a Zeta sizer Nano Series (Malvern, UK) instrument at 37 °C; 10 readings were recorded per sample. The particle size was measured using Image J software.

2.8. SEM and TEM analysis

For the scanning electron microscope (SEM) analysis, diluted dispersed solutions of OFL loaded GG-g-PCL-RA-B-GHS micelle were drop cast onto glass plates and dried. Later, the dried OFL loaded micelle was sputter-coated with Au (thickness ~2 nm) and imaged on an SEM at 5 kV. For Transmission Electron Microscope analysis, diluted and dispersed solutions of GG-g-PCL-RA-B-GHS-OFL nanoparticles were dropped

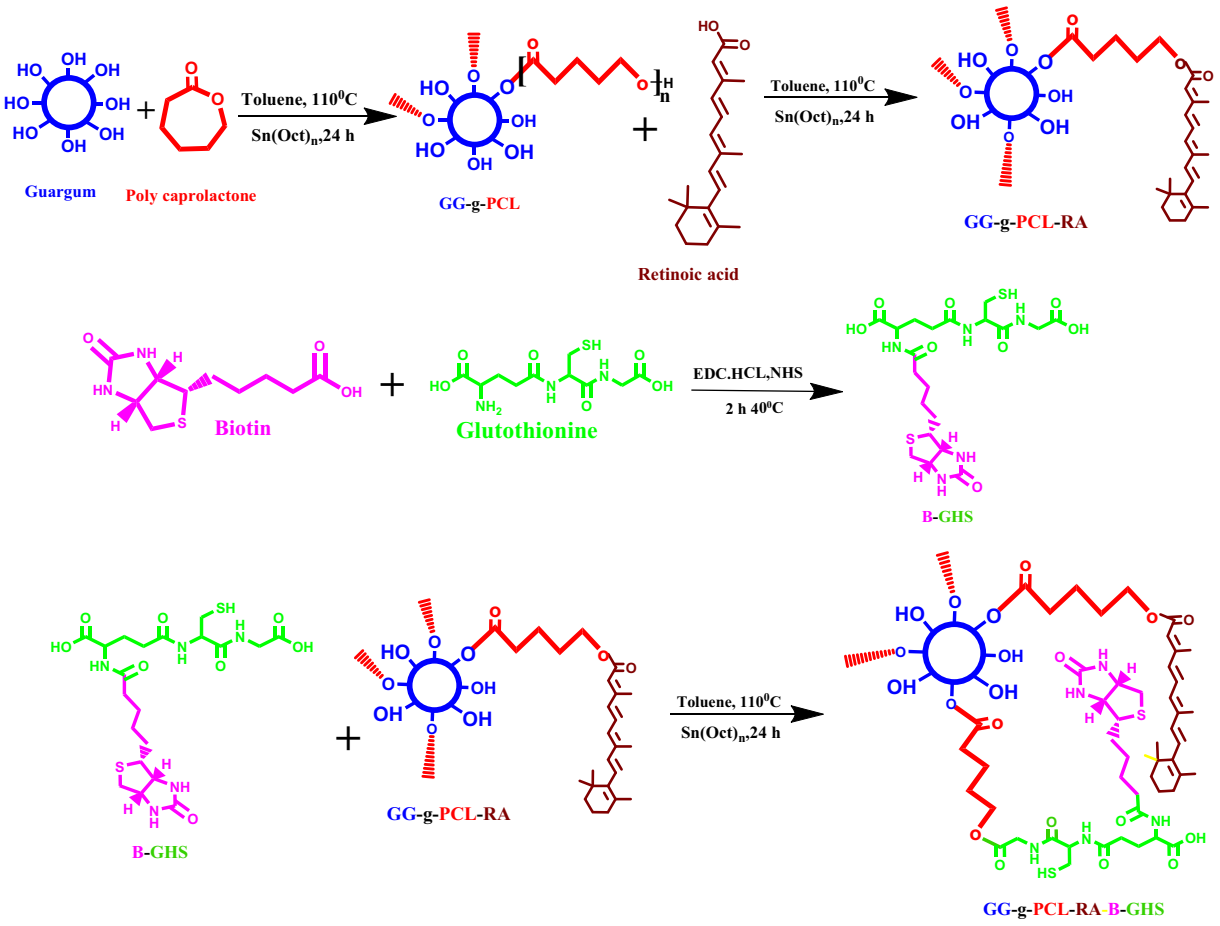

Scheme 1 Schematic representation of GG-g-PCL-RA-B-GHS carrier formation by the chemical reactions.

Table 1 Product yield (%) for the synthesized carrier.

S. No	Name of the polymeric carrier	Weight of the substrate	Product yield (%)
1	GG-g-PCL	0.8244 g	73.0
2	GG-g-PCL-RA	0.1776 g	54.0
3	GG-g-PCL-RA-B-GHS	0.1786 g	66.0
4	OFL loaded GG-g-PCL-RA-B-GHS	0.2800 g	68.0

onto a copper grid (~200 meshes), dried, and observed at 200 kV.

2.9. Fluorescence spectroscopy

Amphiphilic polymers with a suitable hydrophilic/hydrophobic balance can form amicellar structure when exposed to select solvents. The concentration of the amphiphilic polymers when the micellar structure forms is referred to as the criticalmicelle concentration (CMC). Thus the self-aggregating properties and CMC of GG-g-PCL-RA-B-GHS were determined using fluorescence spectroscopy with pyrene as a fluorescent probe. The pyrene solution (3.0 × 10–4 mol/L) in methanol was added to a series of test tubes and evaporated under a nitrogen gas stream to remove the solvents. Then, various GG-g-PCL-RA-B-GHS solutions were added to each test tube in the presence of pyrene at a final concentration of 6.0×10^{-7} mol/L. The solutions were sonicated for 30 min in an ultrasonic bath. Pyrene emission spectra were recorded using a fluorescencespectrophotometer (Shimadzu F-4500, Japan). The probe was excited at 333 nm, and the emission spectra were obtained in the range of 480–540 nm with 1.0 s of integration time. The slit widths for excitation and emission were 10 and 2.5 nm, respectively.

2.10. Swelling studies

The swelling behavior of OFL loaded GG-g-PCL-RA-B-GHS micelle was studied under different pH conditions pH 5.5, 6.8, and7.4 with constant temperature 37 °C and different temperature 27 °C, 37 °C, and 40 °C with constant pH of 7.4. The measurement duration was up to 24 h in order to reach the maximum absorption. The lyophilized OFL loaded GG-g-PCL-RA-B-GHS micellewas pelleted using a hydraulic pelletizer. After recording its dry weight (W_d), the pellet was placed in the corresponding pH solutions in a different time interval. It was then removed from the solution; the surface-adsorbed solution was removed using filter paper wet weight was recorded (W_e). Triplicate samples were analyzed for each

experiment. The swelling ratio was calculated using the following formula

$$\text{Swelling ratio } (\%) = \frac{We - Wd}{Wd} \times 100$$

where W_e weight of the swollen micelle and W_d is the weight of the dry micelle.

2.11. Drug loading and releasing analysis.

OFL loading capacity by the GG-g-PCL-RA-B-GHS micelle was analyzed in UV–Visible spectroscopy analysis (UV-1800, Shimadzu, Japan), λmax value of 287 nm. The drug release rate of OFL from GG-g-PCL-RA-B-GHS was determined by the dialyzing method. The test sample was carried out phosphate buffer saline (PBS) solutions (pH 7.4). Later, the solution was agitated (50 rpm) at 37 °C. Every 30 min time interval, 3 mL of the PBS medium was removed and replaced with fresh PBS. Triplicate samples were analyzed for each experiment. Loading capacity and drug release percentage were calculated through the following equation.

$$LC(\%) = \frac{\text{The total amount of drug} - \text{Free amount of drug}}{\text{weight of the dried micelle}} \times 100$$

$$\text{Drug release } (\%) = \frac{\text{Absorbance value of releasing drug}}{\text{Absorbance value of free drug}} \times 100$$

2.12. Determination of antibacterial activity

2.12.1. Bacterial strains

The bacteria used in this study included gram-positive bacteria (*Bacillus cereus* MTCC430) and gram-negative bacteria (*Salmonella typhi* MTCC733). Both strains were procured from the Microbial Type Culture and Collection, Mumbai, India.

2.12.2. Culture media

Stock cultures were maintained at 4 °C on Luria Broth agar (LB agar). Active cultures of strains for experiments were prepared by transferring a loopful of cells from the stock cultures to test tubes of nutrient broth that were incubated without agitation for 24 h at 37° C. Muller-Hinton (Himedia, Mumbai, India) were used for susceptibility testing.

2.12.3. Antibacterial susceptibility testing

The modified agar well diffusion method of Kavanagh F (1972) was employed (Kavanagh, 1972). By pouring 20 mL of sterile M.H. agar, the culture plates were made ready, and each inoculum suspension was swabbed onto the agar surface. A sterile cork borer (8 mm) has been used for extracting holes in each plate. These plates were marked, and 50 µl of GG, GG-g-PCL, GG-g-PCL-RA, GG-g-PCL-RA-B-GHS, and OFL loaded GG-g-PCL-RA-B-GHS (at a concentration of 1 mg/ml) was aseptically added into the well. Sterile; the tests were carried out by triplicate. Plates were incubated for 24 h at 37 °C, during the activity was manifested by the presence of zone inhibition surrounding the well. The activity was denoted as the mean of the diameter of the inhibition zones (mm).

2.13. Statistical analysis

All experiments were triplicated. The one-way analysis of variance (ANOVA) was used for the statistical analyzing tool. Information isaccounted for as mean ± standard commitments (SD) with a centrality level of $P < 0.005$.

3. Results and discussion

3.1. Synthesis of GG-g-PCL-RA-B-GHS micelle

A targeted drug delivery system was designed to deliver the antibiotic ofloxacin drug to treating ocular diseases. Initially, GG-g-PCL copolymer was synthesized by esterification of ε-caprolactone monomer into the hydroxyl group of guar gum via ring-opening polymerization. Further, the retinoic acid was conjugated with guar gum-grafted polycaprolactone copolymer through condensation of ester bond formation. Biotin's conjugation with the cross-linking of GSH was carried out via a standard amide bond formation using EDC/NHS coupling reagents. Finally, the OFL drug is loadedin the GG-g-PCL-RA-B-GHS micelle by dialysis method. The schematic synthesis of GG-g-PCL-RA-B-GHS was shown in Fig. 1.

3.2. FT-IR analysis

FT-IR analysis was performed to confirm the grafting and conjugation of GG-g-PCL, GG-g-PCL-RA, GG-g-PCL-RA-B-GHS, and OFL loaded GG-g-PCL-RA-B-GHS micelle, B-GHS, and OFL drug results are shown in Fig. 2. Fig. 2 (A) shows the FTIR spectrum of B-GHS and the absorbance of bands appears at 1650 and 1550 cm^{-1}, corresponding to the C—O stretches and —NH bending modes of the amide —CONH— group. Other peaks of Biotin and glutathionewas noticed at 3366 cm^{-1}, 1719 cm^{-1}, 1076 cm^{-1}, 931 cm^{-1} and 3033 cm^{-1}, 2525 cm^{-1}, 543 cm^{-1} respectively (Balan et al., 2012; Kavita et al., 2014), which confirms the biotinylated glutathione conjugation. Fig. 2 (B) shows the FTIR spectrum of free OFL drugs. The characteristic peaks at 3640 cm^{-1} are the characteristic O—H stretching frequencies, and the spectrum at the 2700 cm^{-1} region denote N—H stretching frequencies. The peak at 1606 cm^{-1} was assigned to N—H bending vibration of quinolones. The peak at 1534 cm^{-1} represented the (υCH_2) of the aromatic ring of the OFL. Besides, a strong absorption peak of 1022 cm^{-1} was assigned to the C-F group, and a band at 1214 cm^{-1} suggested the stretching vibration of the oxo group of OFL (Pandya et al., 2010). The expansive vibration around 3439 cm^{-1} is to the corresponding hydroxyl groups of guar gum, and a characteristic signal of the carbonyl groups ester was observed at 1707 cm^{-1} in Fig. 2C (GG-g-PCL). Two other peaks in the range 2875–2922 $cm^{-1}$are obtained, the —CH stretch frequencies of PCL, confirming the grafted GG-g-PCL copolymer (El Assimia et al., 2019). Further, RA conjugation in GG-g-PCL copolymer, a new band that appears in the range of 1707 cm^{-1} to 1735 cm^{-1}, indicates the ester bond formation between retinoic acid and

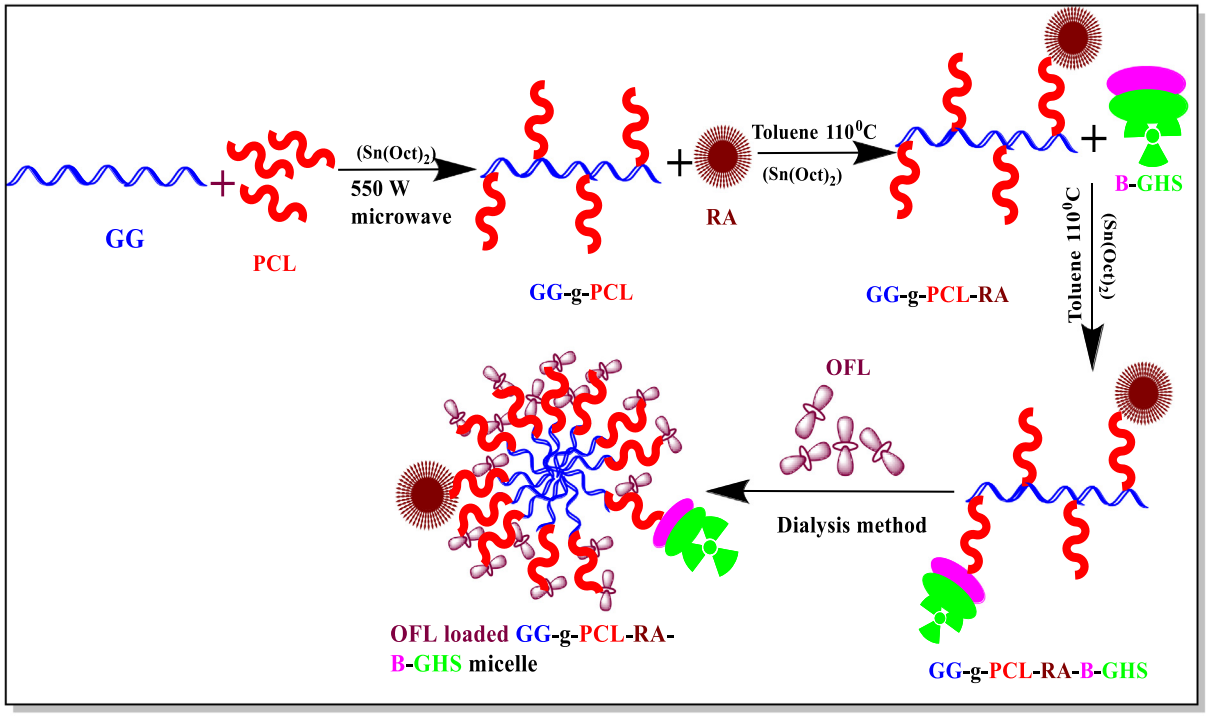

Fig. 1 Graphical representation of GG-g-PCL-RA-B-GHSmicelle formation.

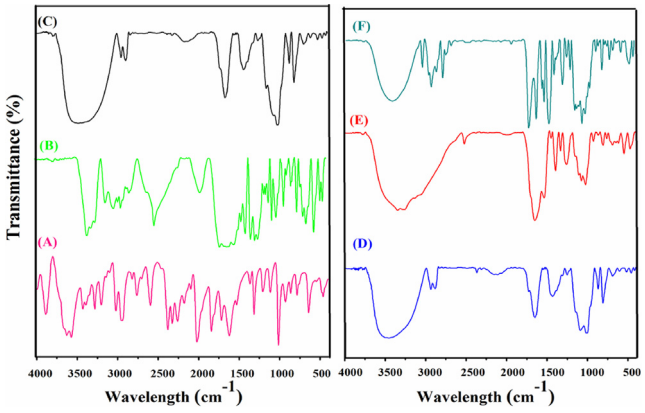

Fig. 2 FT-IR spectrum of (A) B-GHS, (B) OFL DRUG, (C) GG-g-PCL, (D) GG-g-PCL-RA, (E) GG-g-PCL-RA-B-GHS, (F) OFL loaded GG-g-PCL-RA-B-GHS micelle.

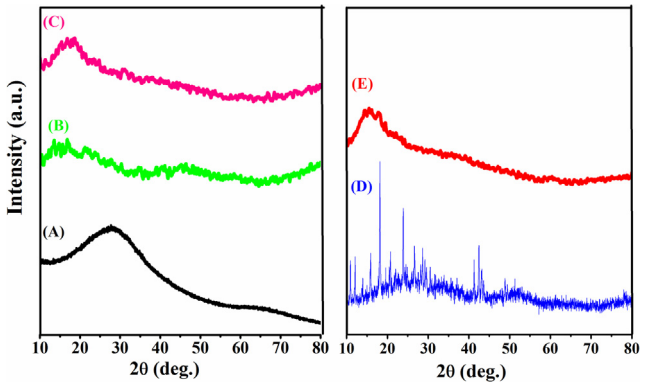

Fig. 3 XRD spectra of (A) GG-g-PCL, (B) GG-g-PCL-RA, (C) GG-g-PCL-RA-B-GHS, (D) OFL drug, and (E) OFL loaded GG-g-PCL-RA-B-GHS.

GG-g-PCL copolymer. The presence of retinol represents the peaks at 2933, 1687 cm^{-1}, 1572 cm^{-1}, 1346 cm^{-1}, 1186 cm^{-1}, 962 cm^{-1} (Ghorbani and Zamanian, 2017). It indicates the bond formation between RA and GG-g-PCL (Fig. 2D). Moreover, GG-g-PCL-RA-B-GHS formation was investigated, and the spectrum is presented in the Fig. 2E. Broadband appeared at 1722 cm^{-1}, ensuring that the ester bond formation between B-GHS and GG-g-PCL-RA groups as the GG-g-PCL-B-GHS micelle. The OFL loaded micelle GG-g-PCL-RA-B-GHS retains all the characteristic peaks of OFL drug that confirms OFL is successfully loaded into the micelle (Fig. 2F).

3.3. XRD analysis

XRD patterns of the GG-g-PCL, GG-g-PCL-RA, GG-g-PCL-RA-B-GHS, OFL, and OFL loaded GG-g-PCL-RA-B-GHS micelle are shown in Fig. 3. The GG-g-PCL demonstrated a broader peak at a 2θ value of 26.20, which indicated the amorphous natureof the polymer (Fig. 3A). Correspondingly, the absence of an intense peak of GG-g-PCL-RA represents theamorphous nature (Fig. 3B).Were, abroad peak at 2θ = 23.20°could be seen in the pattern of GG-g-PCL-RA-B-GHS, related to its amorphous structure (Fig. 3C). Diffraction peaks for pure ofloxacin drug were observed range of 2θ value 10.9°, 13.9°, 18.8°, 20.7°, 21.9°, and 26.6° (Hemant

Gangurde et al., 2011), which indicated the crystalline pattern of OFL drug(Fig. 3D). While these peaks disappeared in the XRD pattern into the OFL loaded GG-g-PCL-RA-B-GHS micelle, demonstrating the amorphousness of the formulation-will enhance the dissolution rate (Fig. 3D). Thus, the own crystalline properties of OFL have improved the fine structure of the polymeric micelle.In amorphous formulations; the polymeric micelle's solubility is increased over the crystalline form due to its high energy state (Jog and Diane, 2017).

3.4. Surface charge, micellar size, and morphology

The zeta potential value of both unloaded and OFL loadedmicelle are found to −10.96 mV and −13.96 mV (Fig. 4A&B). The negative charge value is significantly important for binding into the positive surface of the cell membrane. This could be a possible reason for the higher stability and increase retinal permeability (Min Long et al., 2016). Besides, the average diameter of the particles was found as ~4.5 and ~6.8 nm by the ImageJ software analysis for unloaded and OFL loaded carriers, respectively (Fig. 5).OFL loaded micelles' surface morphology was studied with SEM, and TEM results revealed that the micelles are spherical with smooth surface architecture without any aggregation. The spherical shape of the micelle is suitable for permeability into the ocular system (Nayak and Misra, 2018). No differences were observed between unloaded and OFL loaded micelle in terms of morphology (Fig. 6). The size of micelles to be sufficiently suitable allows them to easily permeate through the tightly packed corneal epithelial cells and junctional complexes and overcome the corneal barrier (Xu et al., 2013). The selected area electron diffraction (SAED) spectrum of unloaded and OFL loaded micelle represents the amorphous nature of them with regular arrangements. It is presented in the inner image of Fig. 6G&H. The results are well agreed with the XRD analysis.

3.5. Critical micelle concentration, micellar drug loading

Critical micelle concentration (CMC) of self-assembly GG-g-PCL-RA-B-GHS amphiphilic polymer to micelle formation was determined via a spectrofluorometer and pyrene used as the fluorescent moiety. As shown in Fig. 7A, the GG-g-PCL-RA-B-GHS polymer self-assembly was anticipated to form as the concentrations increased from 0.001 to 0.010 mg/mL^{-1} proportionately, with a corresponding increase in fluorescence intensity. It illustrates the incorporation of pyrene molecules into the poly (GG-g-PCL-RA-B-GHS) micelle. The I_3/I_1 ratios were virtually unchanged at low micelle concentrations, whereas at higher concentrations, the ratios decreased, indicating self-aggregation of GG-g-PCL-RA-B-GHS polymeric carrier (Fig. 7B). A large increase in the intensity ratio appears above a particular concentration, which shows the onset of micelle formation. It is clear that the CMC value of GG-g-PCL-RA-B-GHS micelle concentration-

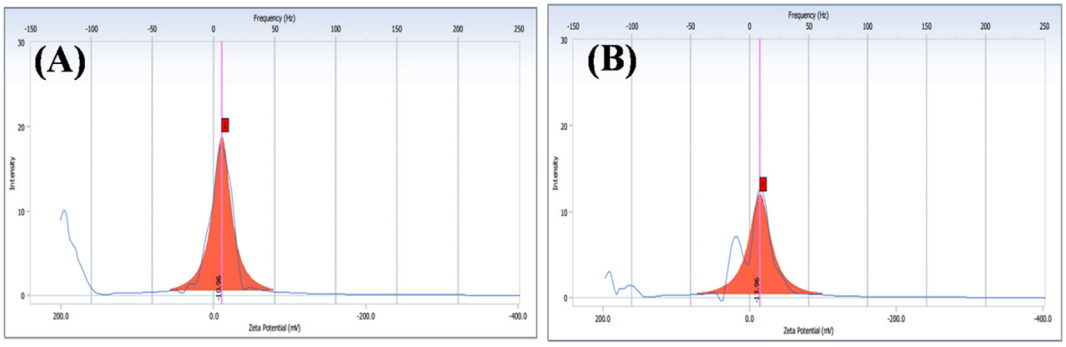

Fig. 4 Zeta potential distribution (A) GG-g-PCL-RA-B-GHS, and (B) OFL loaded GG-g-PCL-RA-B-GHS micelle.

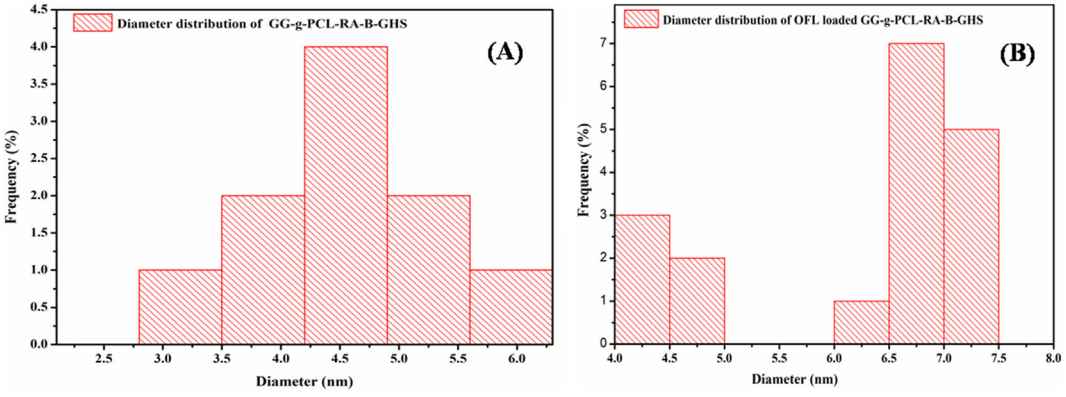

Fig. 5 Particle diameter distributions of (A) GG-g-PCL-RA-B-GHS and (B) OFL loaded GG-g-PCL-RA-B-GHS micelle.

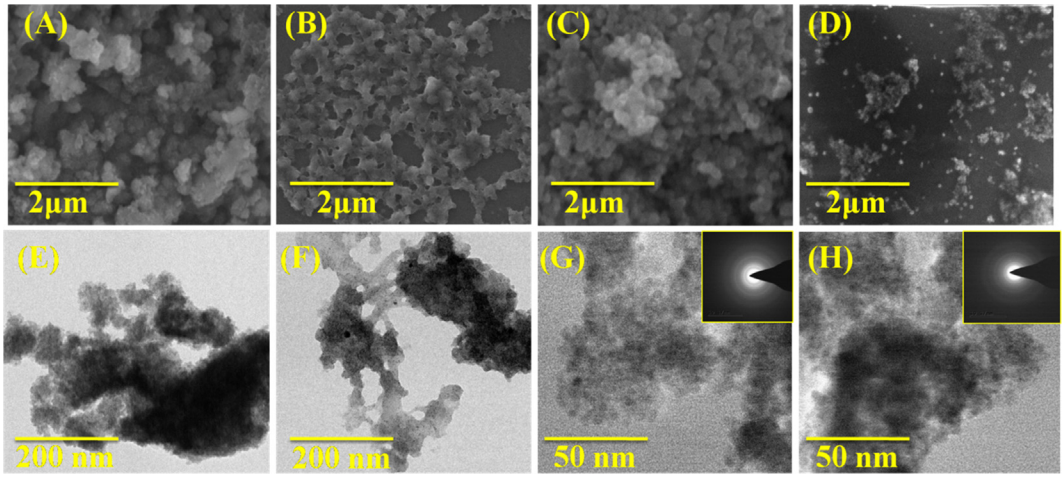

Fig. 6 SEM and TEM images of (A&E) GG-g-PCL, (B&F) GG-g-PCL-RA (C&G), GG-g-PCL-RA-B-GHS micelle, & (D&H) OFL loaded GG-g-PCL-RA-B-GHS micelle, and (G) & (H) Inserted SAED image of unloaded and OFL loaded micelle.

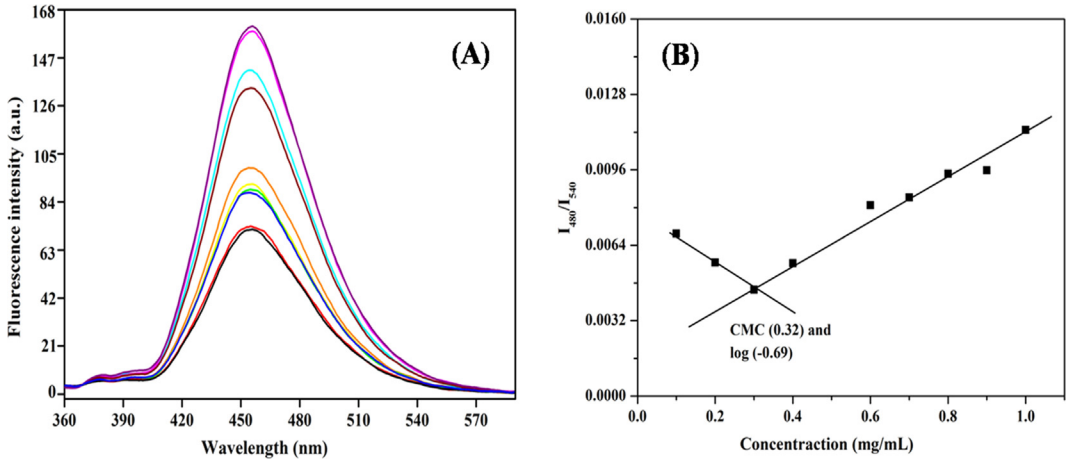

Fig. 7 (A) Fluorescence spectra of GG-g-PCL-RA-B-GHS in dimethyl sulfoxide (DMSO)/water mixtures and pyrene as fluorescent moiety; (B) Determination of the critical micelle concentration of GG-g-PCL-RA-B-GHS micelle formation.

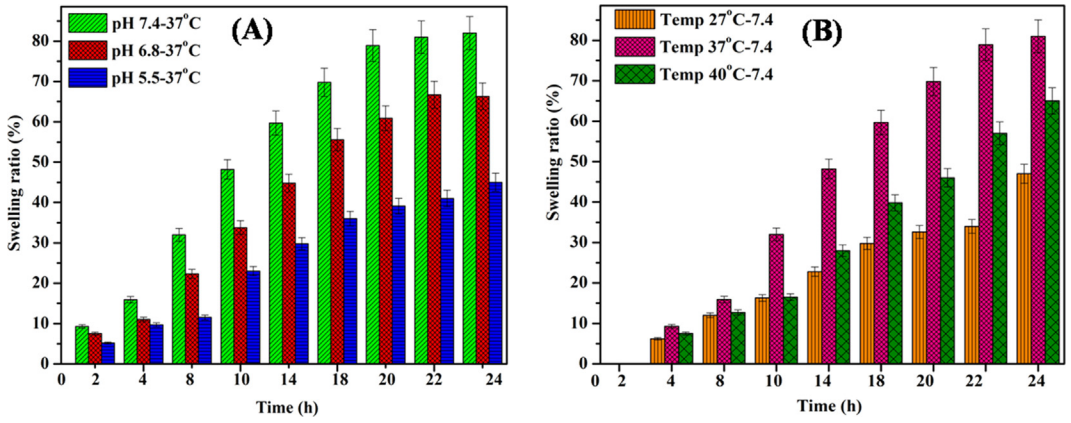

Fig. 8 Swelling behavior of (A) OFL loaded micelle at various buffer solutions 5.5, 6.8 and 7.4 at 37 °C, and (B) OFL loaded micelle at different temperature (27 °C, 37 °C and 40 °C) with constant pH at 7.4.

dependent crossing point of the two tangents, which came out to be was 0.32 μg/mL^{-1} (−0.49 mg/mL), and this value was dependent on the hydrophobic block of PCL.

3.6. Swelling studies

The swelling profile of OFL loaded micelle was carried out in different buffer solutions (pH 5.5, 6.8, and 7.4 at constant temperatures (37 °C) and various temperatures (27 °C, 37 °C, and 40 °C) with stable pH at 7.4 at 24 h. The impact of pH and temperature on the high swelling behavior of OFL loaded micelles was obtained, and it was shown in (Fig. 8A&B). The maximum swelling ratio was observed at pH 7.4 at 37 °C when compared to other buffer solutions (pH 5.5 and 6.6) at 37 °C. Meanwhile, the variation of temperature much more variation was not observed. It confirms that the stability of the carrier system and it not affected the varying temperature. Similarly, the previously reported literature was the evidence of the above facts (Li et al., 2020). Moreover, the unreacted hydroxyl groups are also deprotonated under essential medium, and ester bonds undertake alkaline hydrolysis. Thus, electrostatic repulsion and cross-linked is eruption favor the increase in swelling ratio (Q/Q_0) observed for micelle in primary medium, which means to be tear saline solution (Chatterjee et al., 2020).

3.7. In-vitro release studies

The OFL drug loading capacity of the GG-g-PCL-RA-B-GHS micelle was given in Fig. 9a. The absorbance intensity with λ max value of 287 nm for OFL drug gradually decreased after 60 min from UV–Visible spectroscopic investigation. It indicates the OFL drug-loaded effectively loaded into the GG-g-PCL-RA-B-GHS micelle. Drug loading efficiency was calculated, and it was observed 64.23% by the micelles. Generally, the drug delivery system has limited stability, drug loading capacity, and cost-effectiveness for topical drug delivery (Subrizi et al., 2019). Thus the synthesized GG-g-PCL-RA-B-GHS micelle has a good loading capacity for ocular drug delivery application.

The OFL drug release from the GG-g-PCL-RA-B-GHS micelle was investigated in an ocular pH environment (pH 7.4) and temperature (37 °C). Fig. 9b shows the release profiles of OFL from GG-g-PCL-RA-B-GHS micelle. It shows the controlled drug release's initial burstrelease obeys a diffusion-controlled mechanism. The drug's slow release from the micelles could be attributed to the hydrophobic–hydrophobic interactions between the drug molecules and the micelles' hydrophobic core. In the cumulative drug release studies, the drug release in PBS medium pH 7.4 OFL from GG-g-PCL-RA-B-GHS micelle 88.0% released up to 8 h

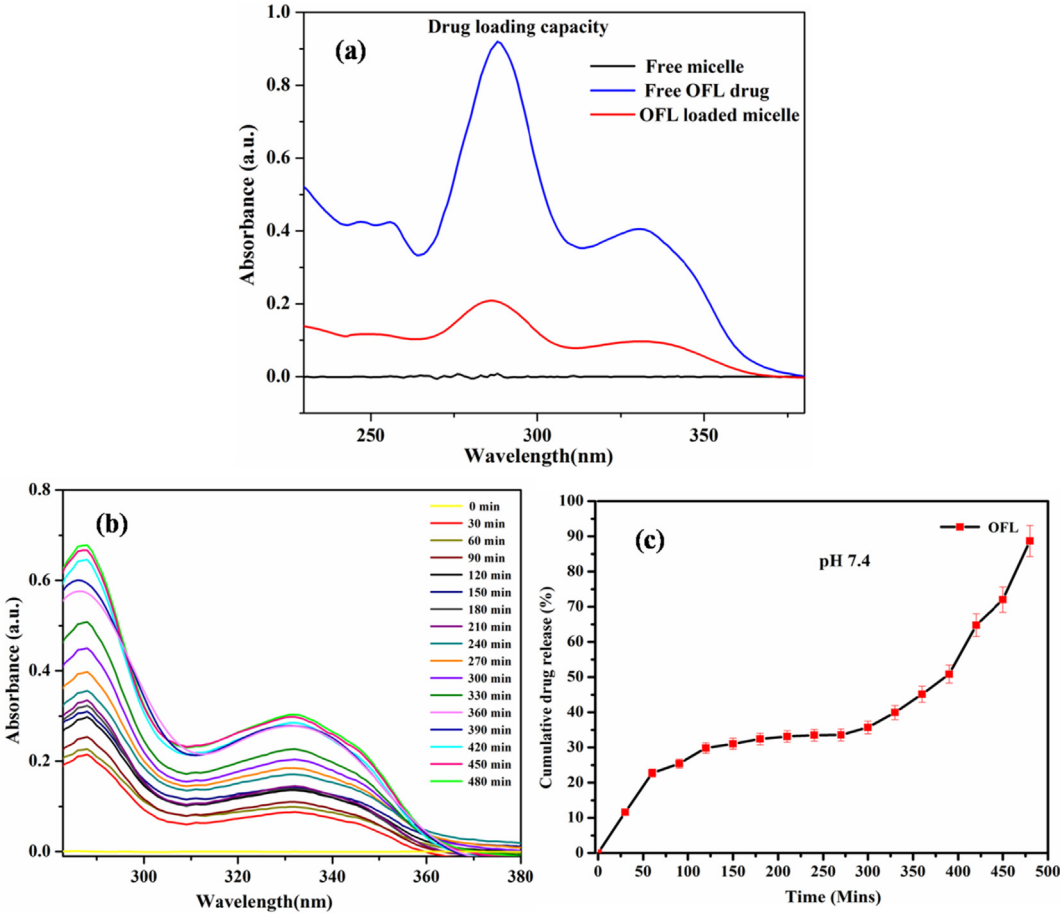

Fig. 9 (a) Loading capacity; (b) *In-vitro* release of OFL from OFL loaded GG-g-PCL-RA-B-GHS micelle at pH 7.4, and (c) Cumulative drug releases.

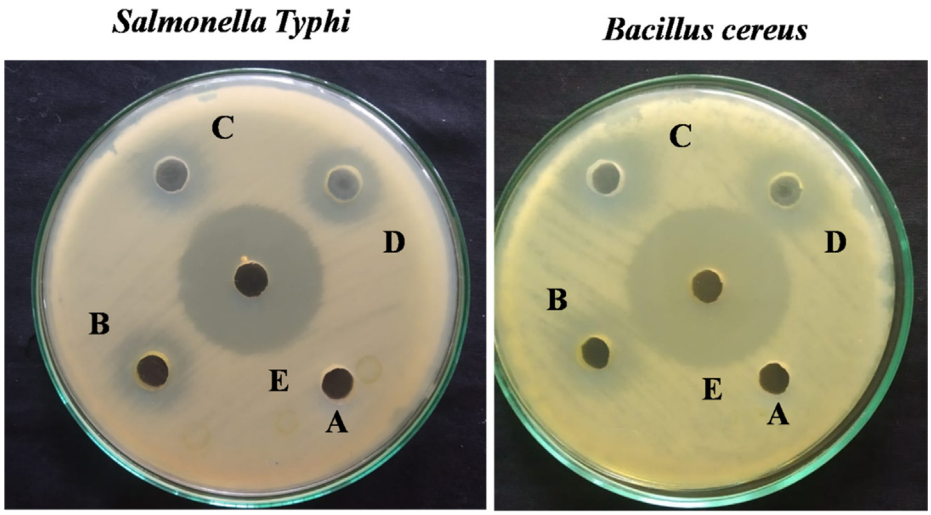

Fig. 10 Antibacterial activity of (A) GG, (B) GG-g-PCL, (C) GG-g-PCL-RA, (D) GG-g-PCL-RA-B-GHS, and (E) OFL loaded GG-g-PCL-RA-B-GHS micelle determined by the discdiffusion technique.

Table 2 Zone of Inhibition (mm) showed by synthesized carrier on the bacteria tested.

S. No	Name of the Carrier	*Salmonella Typhi* (mm ± SD)	*Bacillus cereus* (mm ± SD)
1	GG	0 ± 0	0 ± 0
2	GG-g-PCL	11.30 ± 0.01	14.10 ± 0.00
3	GG-g-PCL-RA	13.20 ± 0.53	14.41 ± 0.54
4	GG-g-PCL-RA-B-GHS	22.20 ± 0.35	18.01 ± 0.58
5	GG-g-PCL-RA-B-GHS-OFL	35.44 ± 0.03	30.18 ± 0.01

(Fig. 9c). These results indicate that the micelle has great potential applications for localized, prolonged ocular residence time and sustained drug release of OFL in a neutral environment.

3.8. Antibacterial activity

Agar well diffusion assay, the preliminary step to screen for antibacterial activity, was performed on the synthesized samples against gram-negative pathogenic bacteria (*Salmonella Typhi*) and gram-positive pathogenic bacteria (*Bacillus cereus*) for 24 h inhibition time (Fig. 10). At the concentration of 1 mg/ml, GG is inactive against both test bacteria. Other synthesized samples showed inhibition zones with the value of *Salmonella Typhi* 11.30 ± 0.01 to 35.44 ± 0.03 *Bacillus cereus* 14.10 ± 0.00 to 30.18 ± 0.01 (Fig. 10, Table 2). The antibacterial behavior of synthesized samples was due to the interactions between the charged micelles and charges present on the bacterial membrane's surface (Hollmann et al., 2018). The OFL loaded GG-g-PCL-RA-B-GHS formulations had a larger zone of inhibitions in comparison to its components.

Further, the GG-g-PCL-RA-B-GHS polymeric micelle and OFL drug chains' contact with the bacterial cell membrane's lipid layer disrupts the cell's protein synthesis. It stops the enzymatic activities required for the survival of the cell (Okur et al., 2014; Umar Aslam khan et al., 2021). The higher inhibition effect represents the synergism between GG-g-PCL-RA-B-GHS micelle and OFL drug compact together to give excellent antibacterial activity.

4. Conclusion

In summary, we have successfully designed and synthesized retina targeting ofloxacin drug-loaded GG-g-PCL-RA-B-GHS micelle. The morphology of GG-g-PCL-RA-B-GHS-OFL was observed as sphere-like morphology through SEM and TEM characterizations. Thus, the spherical-shaped micelle displayed a higher and faster rate of cell penetration. From in-vitro drug release studies, the drug release in a tear fluid physiological environment (PBS, pH 7.4) was observed to be OFL 88.0% in 8 h, and the drug release rate was renewed in a controlled manner to the requirement for prolonged drug delivery. Antibacterial activity of GG-g-PCL-RA-B-GHS-OFL is higher than GG-g-PCL-RA-B-GHS is due to the incorporation of the OFL drug. It observed a good antibacterial activity against both *Salmonella Typhi* and *Bacillus cereus* pathogens. Thus GG-g-PCL-RA-B-GHS-OFL micelle has been potentially used in topical ocular drug delivery applications after the investigation in-vivo and clinical analysis.

CRediT authorship contribution statement

Qiang Shi: Conceptualization, Data curation, Formal analysis, Funding acquisition, Project administration, Resources, Software, Supervision, Validation, Visualization, Writing - original draft, Writing - review & editing. **E.R. Anishiya Chell Daisy:** Investigation, Methodology, Project administration, Resources, Software, Writing - original draft, Writing - review & editing. **Geqiang Yang:** Investigation, Methodology, Writing - original draft, Writing - review & editing. **Jing Zhang:** Investigation, Methodology, Writing - original draft, Writing - review & editing. **Suresh Mickymaray:** Formal analysis,

Project administration, Resources, Software, Writing - original draft, Writing - review & editing. **Faiz Abdulaziz Alfaiz:** Investigation, Methodology, Writing - original draft, Writing - review & editing. **Anand Paramasivam:** Data curation, Funding acquisition, Project administration, Resources, Software, Writing - original draft, Writing - review & editing. **Mariappan Rajan:** Conceptualization, Data curation, Formal analysis, Funding acquisition, Project administration, Resources, Software, Supervision, Validation, Visualization, Writing - original draft, Writing - review & editing.

Declaration of Competing Interest

The authors declare that they have no known competing financial interests or personal relationships that could have appeared to influence the work reported in this paper.

Acknowledgment

M. Rajan is grateful for the financial support under the SERB Research project (F.NO.EEQ/2020/000201), New Delhi, India, and acknowledges the UPE and PURSE programs for the purchase of the TEM, SEM, and FTIR instruments.The authors would like to thank the Deanship of Scientific Research, Majmaah University, Kingdom of Saudi Arabia for research support under the project number: R-2021-52.

References

Agrahari, V., Mandal, A., Pal, D., et al, 2016. A comprehensive insight on ocular pharmacokinetics. Drug Deliv. Transl. Res. 6 (6), 735–754.

Algahtani, M.S., Zaki Ahmad, M., Ahmad, J., 2020. Nanoemulgel for improved topical delivery of retinyl palmitate: formulation design and stability evaluation. Nanomaterials. 10, 848.

Anishiya Chella Daisy, E.R., Naresh, R., Rajan, M., 2020. Retinal photoreceptors targeting SA-g-AA coated multilamellar liposomes micelle system for cytotoxicity and cellular uptake evaluation. J. Liposome Res, 1–35.

Arlappa, N., 2011. Vitamin A deficiency is still a public health problem in India. Indian pediatr. 48, 853–854.

Balan, V., Ionelpopa, M., Butnaru, M., 2012. Biotinylated chitosan-based spions with potential in blood contacting applications. J. Nanopart Res. 14, 730.

Bhowmik, M., Kumari, P., Sarkar, G., et al, 2013. Effect of xanthan gum and guar gum on in situ gelling ophthalmic drug delivery system based on poloxamer-407. Int. J. Biol. Macromol. 62, 117–123.

Blomhoff, R., 1991. Vitamin A metabolism: new perspectives on absorption, transport, and storage. Physiol Rev. 71 (4), 951–990.

Chatterjee, S., Upadhyay, P., Mishra, M., et al, 2020. Advances in chemistry and composition of soft materials for drug releasing contact lenses. RSC Adv. 10, 36751–36777.

Djamila, A., Kamel, A., Philippe, P., et al, 2013. Recent advances in ocular drug delivery. Drug Dev. Ind. Pharm. 39 (11), 1599–1617.

El Assimia, T., Blazicb, R., kadibc, A., et al, 2019. Synthesis of poly(ε-caprolactone)-grafted guar gum by surface-initiated ring opening polymerization. Carbohydr. Polym. 220, 95–102.

Ganea, E.M., Harding, J.J., 2006. Glutathione-related enzymes and the eye. Curr. Eye Res. 31 (1), 1–11.

Gaudana, R., Ananthula, H.K., Parenky, A., et al, 2010. Ocular drug delivery. AAPS J. 12 (3), 348–360.

Ghorbani, F., Zamanian, A., et al, 2017. Effects of pore orientation on in-vitroproperties of retinoic acid-loaded PLGA/gelatin scaffolds for artificial peripheral nerve application. Mater. Sci. Eng. C.77, 159–172.

Hemant Gangurde, H., Mayur Chordiya, A., Tamizharasi, S., et al, 2011. Formulation and evaluation of sustained release bioadhesive tablets of Ofloxacin using 32 factorial designs. 1(3), 148-56.

Hollmann, A, Martinez, M., Maturana, P., et al, 2018. Antimicrobial peptides: interaction with model and biological membranes and synergism with chemical antibiotics. Front Chem. 6, 204.

Jitendra, B.N., Sagar, R., Pardeshi, R.P., et al, 2020. Mucoadhesive micro-/nano micelles in ophthalmic drug delivery: an overview. BioNanoScience. 10, 564–582.

Jog, R., Diane, J., 2017. Pharmaceutical amorphous nanoparticles. Pharm. Sci. 106, 39–65.

Kavanagh, F., 1972. Analytical microbiology. Kavanagh F (ed). Vol.11, Academic Press, Newyork & London.

Kavita, A.N., Singh, K., Kumar, S., et al, 2014. Glutathione-assisted synthesis of star-shaped zinc oxide nanostructures and their photoluminescence behavior. J. Lumin. 149, 112–117.

Khare, A., Grover, K., Pawar, P., et al, 2014. Mucoadhesive polymers for enhancing retention in ocular drug delivery: a critical review. Rev. Adhes. 2 (4), 467–502.

Kong, B., Mi, S., 2016. Electrospun scaffolds for corneal tissue engineering: a review. Materials (Basel). 9 (8), 614.

Kushwaha, S.K., Saxena, P., Rai, A., 2012. Stimuli sensitive hydrogels for ophthalmic drug delivery: A review. Int. J. Pharm. Investig. 2 (2), 54–60.

Leichner, C., Jelkmann, M., Bernkop-Schnürch, A., 2019. Thiolated polymers: bioinspired polymers utilizing one of the most important bridging structures in nature. Adv. Drug Deliv. Rev. 151–152, 191–221.

Li, B., Wang, J., Gui, Q., et al, 2020. Drug-loaded chitosan film prepared via facile solution casting and air-drying of plain water-based chitosan solution for ocular drug delivery. Bioact. Mater. 5, 577–583.

Li, M., Zhang, W., Wang, B., et al, 2016. Ligand-based targeted therapy: a novel strategy for hepatocellular carcinoma. Int. J. Nanomed. 11, 5645–5669.

Min Long, Y., Chen Zhao, X., Clermont, A.C., et al, 2016. Negatively charged silver nanoparticles cause retinal vascular permeability by activating plasma contact system and disrupting adherens junction. Nanotoxicology. 10 (4), 501–511.

Nayak, K., Misra, M., 2018. A review on recent drug delivery systems for posterior segment of eye. Biomed. Pharmacother. 107, 1564–1582.

Ohkura, Y., Ichi, S., Masanori, et al., 2010.Blood to retina transport of biotin via Na+ dependent multivitamin transport (SWVT)at the inner blood-retinal barrier. Exp. Eye Res. 91(3), 387–392.

Okur, N., Gokce, E.H., Ozer, O., et al, 2014. Preparation and in vitro-in vivo evaluation of Ofloxacin loaded ophthalmic nano structured lipid micelles modified with chitosan oligosaccharide lactate for the treatment of bacterial keratitis. Eur. J. Pharm. Sci. 63, 204–215.

Pandya, S.J., Bhalekar, M.R., Harinarayana, D., et al, 2010. Preparation and characterization of light sensitive ofloxacin complexes under accelerated condition. Interjpharm Res. 2, 28–32.

Patel, A., Cholkar, K., Agrahari, V., et al, 2013. Ocular drug delivery systems: An overview. World J. Pharmacol. 2 (2), 47–64.

Priyanka, P., Sandeep, A., Pravin, P., 2012. Ocular drug delivery system: a reference to natural polymers. Expert Opin. Drug Deliv. 9 (7), 837–861.

Rajan, M., Pradeepkumar, P., Rajendran, N.K., et al, 2018. Deep eutectic solvent-mediated FA-g-β-alanine-co-PCLdrug micelle for sustainable and site-specific drug delivery. ACS Appl. Biol. Mater., 1–49.

Sahoo, S.K., Dilnawaz, F., Kirshnakumar, S., 2008. Nanotechnology in ocular drug delivery. Drug Discov Today. 13 (3–4), 144–151.

Sharma, S., Sahu, K., 2017. Simultaneous determination of Nitazoxanide and Ofloxacin in pharmaceutical preparations using UV-

spectrophotometric and high performance thin layer chromatography methods. Arab. J. Chem. 10, S62–S66.
Sommer, A., 1983. Effects of vitamin A deficiency on the ocular surface. Ophthalmology 90 (6), 592–600.
Song, R., Murphy, M., Li, C., 2018. Current development of biodegradable polymeric materials for biomedical applications. Drug Des. Devel. Ther. 12, 3117–3145.
Soppimath, K.S., Kulkarni, A.R., Aminabhavi, T.M., 2001. Chemically modified polyacrylamide-*g*-guar gum-based cross-linked anionic microgels as pH-sensitive drug delivery systems: preparation and characterization. J. Control. Release 75 (3), 331–345.
Subrizi, A., Del Amo, E.M., Vlakh, V.K., et al, 2019. Design principles of ocular drug delivery systems: importance of drug payload, release rate, and material properties. Drug Discovery Today 24 (8), 1446–1457.
Tan, B.L., Norhaizan, M.E., Liew, W.P., et al, 2018. Antioxidant and oxidative stress: A mutual interplay in age-related diseases. Front. Pharmacol. 9, 1162.
Tan, J.C.K., Tat, L.T., Coroneo, M.T., 2016. Treatment of partial limbal stem cell deficiency with topical interferon α-2b and retinoic acid. Br. J. Ophthalmol. 100, 944–948.
Tiwari, A., Prabaharan, M., 2010. An amphiphilic nanomicelle based on guar gum-graft-Poly(ε-caprolactone) for potential drug-delivery applications. J. Biomater. Sci. 21, 937–949.
Umar Aslam khan, M., Haider, Sajjad, Abdul kadir, M.R., et al, 2021. Development of porous, antibacterial and biocompatible GO/n-HAp/bacterial cellulose/β-glucan biocomposite scaffold for bone tissue engineering. 14(2), 102924.
UstundagOkur, N., Homan Gokce, E., Egrilmez, S., et al, 2014. Novel ofloxacin-loaded microemulsion formulations for ocular delivery. J. OculPharmacolTher. 30 (4), 319–332.
Wang, F., Guob, Y., Wang, W., 2020. Development of nano-tricalcium phosphate/polycaprolactone/platelet-rich plasma biocomposite for bone defect regeneration. Arab. J. Chem. 13 (9), 7160–7169.
XiuRen, W., Han, J., Uhm, S., et al, 2015. Recent development of biotin conjugation in biological imaging, sensing, and target delivery. Chem. Commun. 51, 10403–10418.
Xu, Q., Kambhampati, S.P., Kannan, R.M., 2013. Nanotechnology approaches for ocular drug delivery. Middle East Afr. J. Opthalmol. 20 (1), 26–37.